# Continuous modulation of charge-spin conversion by electric field in $Pt/Co_2FeSi/Pb(Mg_{1/3}Nb_{2/3})O_3$-$Pb_{0.7}Ti_{0.3}O_3$ heterostructures

Yibing Zhao(赵逸冰)[1,2,†], Xiaoxiao Fang(方晓筱)[1,2,†], Zhirui Wang(王志睿)[1,2], Miao Cheng(程淼)[1,2]
Yongjia Tan(谭永嘉)[1,2], Dongxiong Wei(韦东雄)[1,2], Changjun Jiang(蒋长军)[1,2], and Jinli Yao(幺金丽)[1,2,‡]

[1] *Key Laboratory for Magnetism and Magnetic Materials (Ministry of Education), Lanzhou University, Lanzhou* 730000, *China*
[2] *Key Laboratory of Special Function Materials and Structure Design (Ministry of Education), Lanzhou University, Lanzhou* 730000, *China*

(Received 24 July 2022; revised manuscript received 12 January 2023; accepted manuscript online 13 January 2023)

The half-metallic Heusler alloy $Co_2FeSi$ is an ideal material in spintronic devices due to its higher spin polarization, higher Curie temperature and lower damping parameters. In this work, the dynamic magnetism of $Co_2FeSi$ is modulated by electric field and it is demonstrated that the charge-spin conversion efficiency $\xi$ is continuous and controllable by the electric field. We further find an extremely high $\xi$ in ferromagnetic/ferroelectric (FM/FE) heterostructures, which could be ascribed to interfacial effect in FM/FE interface. Moreover, we investigate that the charge-spin conversion efficiency varies with the electric field in a butterfly-like behavior, which accords with the *S*–*E* curve of $Pb(Mg_{1/3}Nb_{2/3})O_3$-$Pb_{0.7}Ti_{0.3}O_3$(PMN-PT) and could be attributed to strain effect. The modulation of charge-spin conversion efficiency in FM/FE heterostructures via electric field presents a profound potential for next-generation spintronic devices and applications of current-induced magnetization switching.

**Keywords:** Heusler alloy, electric-field modulation, strain effect, Rashba effect

**PACS:** 67.30.er, 67.80.dk, 75.50.–y, 75.70.–i **DOI:** 10.1088/1674-1056/acb2c0

## 1. Introduction

The growing demand for high-speed information reading-writing and high-efficiency information storage increases rapidly with fast development of information technology. The effective implementation of modulating magnetization is one of the significant topics of spintronics. The current-induced magnetization switching via spin–orbit torques (SOTs) generated by spin current is an effective method to realize magnetic random memory (MRAM), highly endurable spin logic devices, and nonvolatile functionality.[1] Traditionally, two main mechanisms are considered to generate spin current: the spin Hall effect[2] (SHE) and the interfacial Rashba effect.[3] The spin Hall effect originates from the strong spin–orbit coupling in heavy metal materials. While the charge current flows in the *x*-direction through the ferromagnetic/heavy metal (FM/HM) bilayer, the SHE caused by the strong spin–orbit coupling in the heavy metal converts it into spin current polarized along the *y*-direction, and the spin current is generated and injected into the adjacent ferromagnetic layer, where the magnetization will be affected by an in-plane damping-like torque $\tau_{DL} \propto m \times (y \times m)$. In addition, the Rashba effect roots in inversion-symmetry breaking and commonly in interface system.[4] An electric field $E$ is generated along the direction of the symmetry breaking due to the spin–orbit interaction. The spin–orbit coupling at the interface causes the conduction electrons' magnetic moment to polarize along $E \times p$ and results in the spin accumulation on the interface, which generates a field-like torque $\tau_{FL} \propto m \times y$ acting on the ferromagnetic layer's magnetization.[5–8] Generally, the Rashba effect is described by the Hamiltonian $H_r = \alpha_R(E \times p) \cdot \sigma/\hbar$, where $\alpha_R$ is the Rashba coefficient.[9] The Rashba field can be calculated by $H_Z = 2\alpha_R k_F/g\mu_B$, where $k_F$ and $g$ are the Fermi wave vector and $g$-factor of the carriers in the conduction channel, respectively.[9] In addition, the charge current generates the Oersted field which creates an oscillating torque acting on the ferromagnetic layer's magnetization and drives it into precession as well.

Generally, the magnitude of charge-spin conversion could be modulated by varying the internal properties like thickness and species of HM/FM bilayers in conventional HM/FM system. A great number of NM metals, such as Pt, Au,[10] Pd,[11,12] $\beta$-Ta,[13] and Ru,[14] have been extensively as the source of spin current when in contact with an FM. The modulation of charge-spin conversion via external method draws great attention, where electric-field modulation is regarded as an effective method. According to the reports, electric field-induced piezoelectric strain can realize an effective modulation of the magnetic anisotropy, magnetic domain structure and the dynamical properties of in-plane films.[15–17] Experimental attempts have been made to explore the effect of electric fields on charge-spin conversion. Lv *et al.*[18] provided a method of SOTs manipulation compatible with field-

†They contributed equally to this work.
‡Corresponding author. E-mail: yaojl@lzu.edu.cn

© 2023 Chinese Physical Society and IOP Publishing Ltd 

effect semiconductor devices based on two-dimensional transition metal dichalcogenides (2D-TMD) materials. Filianina *et al.*[19] investigated the strain response of current-induced SOTs in perpendicularly magnetized W/CoFeB/MgO layers grown on piezoelectric substrates, which demonstrated that the in-plane strain of different properties and magnitude could lead to distinctly different variations of field-like and damping-like torques. Cai *et al.*[20] made great contributions in controlling the spin orbit torque in FM in the hybrid FM/FE structure by electric field, and utilized the magnetization switching without an external magnetic field. Moreover, the half metallic Heusler alloy $Co_2FeSi$ is an ideal material for spin-injected semiconductor devices owing to its high Curie temperature (1100 K),[21,22] low damping parameter as well as low relaxation time in magnetization switching.[23] Thus, it is necessary to investigate the electric-field modulation of charge-spin conversion in $Co_2FeSi$.

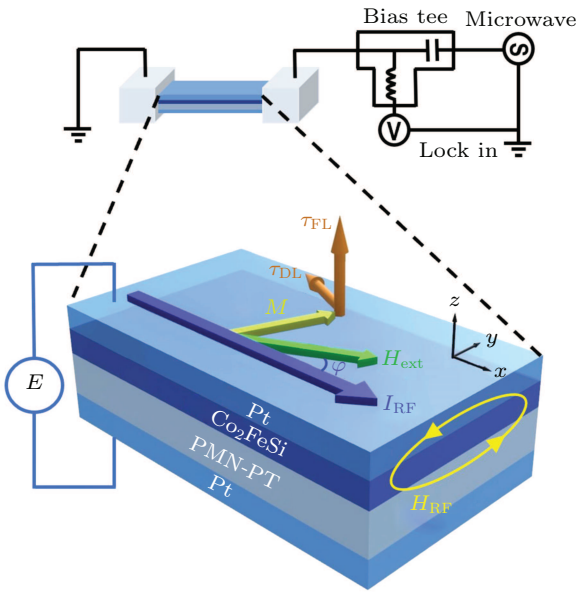



**Fig. 1.** (a) Schematic circuit of ST-FMR measurement. (b) Schematic diagram of structure and electric field modulation of Pt/$Co_2FeSi$/PMN-PT films.

In this work, the electric field continuous modulation of charge-spin conversion efficiency $\xi$ in $Co_2FeSi$ thin films deposited on the ferroelectric substrates PMN-PT is investigated. The $\xi$ is determined by the ratio of the symmetric component and antisymmetric component through spin-torque ferromagnetic resonance (ST-FMR). With a large electric field applied, the $\xi$ is significantly modulated in a continuous manner. In particular, it is interesting to find that the trend of $\xi$ with electric field $E$ obeys a butterfly-like behavior and coincides with the $S$–$E$ curve of the PMN-PT, which can be ascribed to the piezostrain effect.

## 2. Experiment

The $Co_2FeSi$/Pt thin film was grown on a (001)-oriented PMN-PT substrate whose thickness is 0.4 mm by magnetron sputtering. In order to remove surface contamination before deposition, we pre-annealed the substrate at 350 °C for 1 h. The Pt(5 nm)/$Co_2FeSi$(10 nm)/PMN-PT/Pt(100 nm) structure was prepared 100 nm Pt grown on the rear side of the substrate with the same Pt sputtering conditions as the electrode. A vertical bias electric field was applied to the Pt(5 nm)/$Co_2FeSi$(10 nm)/PMN-PT/Pt(100 nm) structure by using a Keithley 2410 direct current (dc) power source. Figure 1(a) shows the schematic circuit of the ST-FMR measurement. The bias tee allows us to measure the dc voltage while applying a microwave current. During the ST-FMR measurement, a microwave current with certain power (30 dBm) and frequency is exerted along the length direction of the film and a magnetic field $H_{ext}$ is applied along the film plane for sweeping. The lock-in amplifier is used to measure the voltage signal $V_{DC}$ along the length of the film. Figure 1(b) shows the schematic structure and electric field modulation of the Pt/$Co_2FeSi$/PMN-PT films.

## 3. Results and discussion

The charge current in the FM/HM could be converted into spin current through the SHE or the interfacial Rashba effect. The generated spin current will affect the magnetization of the ferromagnetic layer in the form of SOTs and drive it into precession.[24,25] The radio frequency and the magnetic field meet the resonance condition and can be expressed as[26]

$$f = \frac{\gamma}{2\pi}\sqrt{H_r(H_r+\mu_0 M_{eff})}, \tag{1}$$

where $\mu_0$ is the permeability in vacuum, and $M_{eff}$ is the effective saturation magnetization of $Co_2FeSi$. We primarily consider two types of current-induced spin–orbit torques, the field-like torque $\tau_{FL}$ and damping-like torque $\tau_{DL}$. The Landau–Lifshitz–Gilbert equation incorporating the above two spin–orbit torques is presented as follows:[27]

$$\begin{aligned}\frac{d\boldsymbol{m}}{dt} &= -\gamma \boldsymbol{m}\times\boldsymbol{H}_{eff} + \alpha \boldsymbol{m}\times\frac{d\boldsymbol{m}}{dt} + \gamma\tau_{FL}\boldsymbol{m}\times\boldsymbol{\sigma} \\ &\quad + \gamma\tau_{DL}\boldsymbol{m}\times(\boldsymbol{\sigma}\times\boldsymbol{m}) - \boldsymbol{m}\times\boldsymbol{H}_{RF},\end{aligned} \tag{2}$$

where $\gamma$ is the gyromagnetic ratio, $\alpha$ is the Gilbert damping coefficient, $\boldsymbol{H}_{ext}$ is the applied external magnetic field, $\boldsymbol{H}_{eff}$ is the effective magnetic field along with the applied external magnetic field, and $\sigma$ is the direction of the injected spin moment; $\tau_{DL}$, $\tau_{FL}$, and $\boldsymbol{H}_{RF}$ represent the damping-like torque, field-like torque, and Oersted field, respectively. We studied the possible spin–orbit torques in the heterostructure by ST-FMR measurements. The ST-FMR resonance signal can be presented as a superposition of symmetric and antisymmetric signals. Therefore, the dc signal $V_{DC}$ measured by ST-FMR is fitting with the following equation:[28]

$$V_{DC} = V_A\frac{\Delta H(H-H_r)}{(H-H_r)^2+\Delta H^2} + V_S\frac{\Delta H^2}{(H-H_r)^2+\Delta H^2}, \tag{3}$$

where $V_A$ and $V_S$ are the intensities of the antisymmetric and symmetric signal, respectively. $\Delta H$ is the linewidth of the ST-FMR signal, and $H_r$ is the resonance field.

The charge-spin conversion efficiency determined by the ratio of symmetric and antisymmetric amplitudes in the resonance signal is described by the parameter $\xi$,[27]

$$\xi = \left|\frac{J_S}{J_C}\right| = \frac{V_S}{V_A}\frac{e\mu_0 M_S t_{FM} t_{HM}}{\hbar}\sqrt{1+\frac{M_{eff}}{H_r}}, \tag{4}$$

where $e$ is the electronic charge, $\mu_0$ is the permeability in vacuum, $M_S$ is the saturation magnetization of $Co_2FeSi$, $t_{FM}$ is the thickness of $Co_2FeSi$, $t_{HM}$ is the thickness of Pt, and $\hbar$ is the reduced Planck constant. $M_{eff}$ is the effective saturation magnetization of $Co_2FeSi$.

For the Pt(5 nm)/$Co_2FeSi$(10 nm)/PMN-PT/Pt(100 nm) films, we performed ST-FMR measurements by varying the frequency of the microwave at the certain power of 30 dBm, where the angle $\varphi$ between external magnetic field $H_{ext}$ and microwave current is fixed at 45°. By fitting the above data, we obtained the resonance spectra in the sample at various frequencies in the unpolarized state, as shown in Fig. 2(a). The efficiency $\xi$ of charge-spin conversion at different frequencies was calculated by Eq. (4), as shown in Fig. 2(b). The average value of the charge-spin conversion efficiency at different frequencies is about 0.811. In general, the charge spin conversion efficiency caused by the SHE is smaller than Rashba effect. In previous reports, the $\xi$ of Pt in Pt (6 nm)/Py (4 nm) bilayers at room temperature was obtained to be 0.056,[27] and the efficiency of Ta in CoFeB (4 nm)/Ta (8 nm) bilayers was around 0.15,[29] while the maximum $\xi$ observed in the $\beta$-phase W/CoFeB bilayer by ST-FMR measurements for heavy metal was 0.3.[30] However, large $\xi$ presented the Rashba effect very likely. For example, a large spin Hall angle of $6.3 \pm 1$ at room temperature was demonstrated in the two-dimensional electron gas on the interface such as the $SrTiO_3/LaAlO_3$ system, which was several orders of magnitude higher than the $\xi \sim 0.06$–$0.3$ for heavy metals like Pt, Ta, and W.[31] In addition, high $\xi \sim 0.43$–$3.5$ due to strong Rashba effect was also observed in the emerging topological insulator $Bi_2Se_3$.[32,33] In the Pt/$Co_2FeSi$/PMN-PT system, the strong Rashba effect exists in FM/PMN-PT interface since their structure-inversion symmetry is naturally broken,[34] which can be regarded as the source of a large charge spin conversion efficiency.

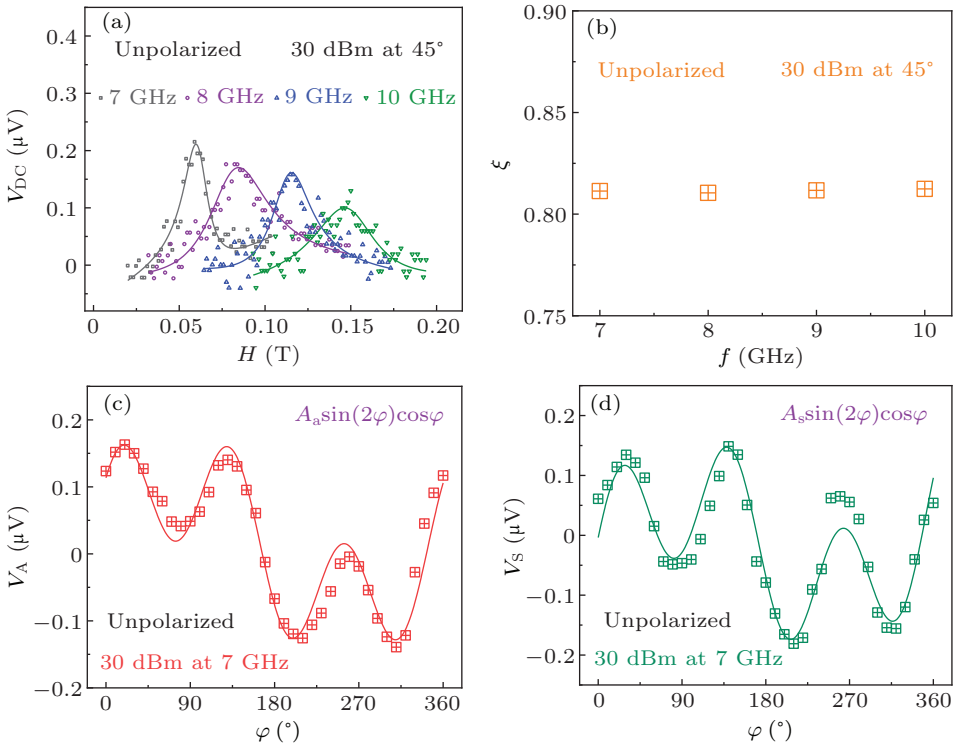



**Fig. 2.** (a) ST-FMR resonance signal $V_{DC}$ of Pt/$Co_2FeSi$/PMN-PT measured in the unpolarized state. (b) Frequency dependence of the charge-spin conversion efficiency $\xi$. [(c), (d)] Angular dependence of the ST-FMR antisymmetric linear component $V_A$ and the symmetric linear component $V_S$ with respect to the in-plane magnetic field angle $\varphi$ with the microwave frequency of 7 GHz and the power of 30 dBm.

To explore the origin of the torques in Pt/$Co_2FeSi$/PMN-PT, we studied the angular dependence of the ST-FMR signal in the applied external magnetic field. In the unpolarized state, we determined the ST-FMR measurements by selecting the angle $\varphi$ between the applied magnetic field and the current varying from 0° to 360° at 10° intervals, when the magnetic field frequency was 7 GHz and the microwave power was 30 dBm. We obtained the dc signal $V_{DC}$ by spin rectification. By fitting the ST-FMR spectrum with Eq. (3), the dependence between the antisymmetric resonance amplitude $V_A$, symmetric amplitude $V_S$ and angle $\varphi$ were obtained, as shown in Figs. 2(c) and 2(d). $V_A$ and $V_S$ can be fitted

by the equation $V_{S(A)} = A_{s(a)} \sin 2\varphi \cos\varphi$. The antisymmetric and symmetric components correspond to the out-of-plane torque and in-plane torque, respectively. Generally, the AMR of $Co_2FeSi$ follows the trend of $\sin(2\varphi)$, while the current-induced torques (anti-damping torque and field-like torque) follow $\cos(\varphi)$ behavior.[27]

To investigate the effect of electric field on charge-spin conversion, we conducted ST-FMR measurements on Pt/$Co_2FeSi$/PMN-PT by varying the electric field at 7 GHz. In order to ensure the stability of the measurements, the sample was polarized several times under different positive and negative electric fields before the measurements. Figures 3(a) and 3(b) illustrate the ST-FMR spectra obtained by measurements at 30 dBm and 7 GHz with the electric fields of +0 kV/cm, +3.75 kV/cm, −0 kV/cm, and −3.75 kV/cm, where +0 kV/cm and −0 kV/cm represent the remnant polarization states under positive and negative electric fields, respectively.

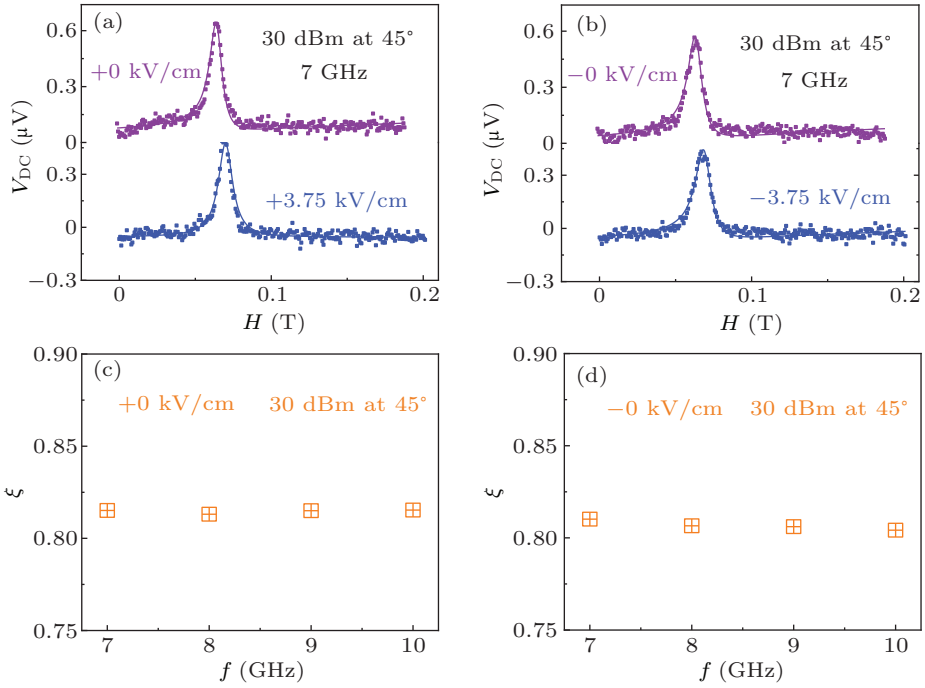



**Fig. 3.** (a), (b) ST-FMR spectrum at 7 GHz, 30 dBm, with electric fields: (a) +0 kV/cm and +3.75 kV/cm, (b) −0 kV/cm and −3.75 kV/cm. (c), (d) Charge-spin conversion efficiency $\xi$ at electric fields: (c) +0 kV/cm and (d) −0 kV/cm.

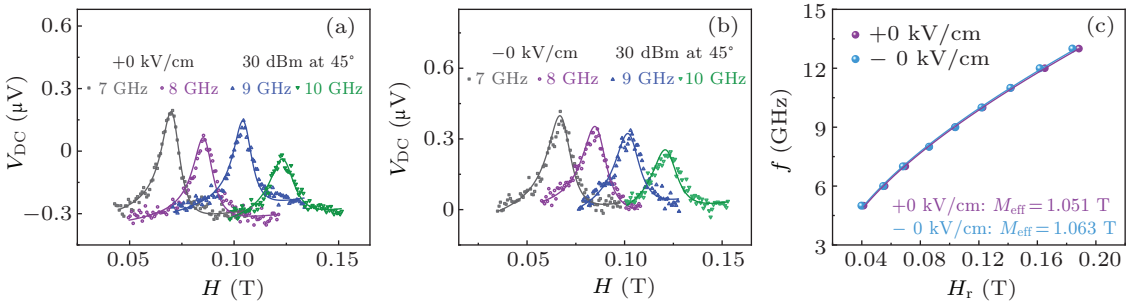



**Fig. 4.** (a) ST-FMR resonance signal $V_{DC}$ of Pt/$Co_2FeSi$/PMN-PT measured at electric fields of +0 kV/cm and (b) −0 kV/cm. (c) Dispersion relation between the resonant field $H_r$ and frequency at electric fields of +0 kV/cm and −0 kV/cm.

We performed the ST-FMR measurements by varying the frequency of the microwave in the positive and negative remnant polarization states, and the signal was fitted according to Eq. (4) to obtain the charge-spin conversion efficiency in the remnant polarization state, as illustrated in Figs. 3(c) and 3(d). The charge-spin conversion efficiencies in the positive ($E = +0$ kV/cm) remnant polarization state ($\xi = 0.817$) is similar to that ($\xi = 0.806$) in the negative ($E = 0$ kV/cm) remnant polarization state, which implies similar in-plane piezoelectric strain in the PMN-PT for the positive and negative remnant polarization state.

Figures 4(a) and 4(b) give the ST-FMR spectra obtained at different frequencies measured at electric fields of +0 kV/cm and −0 kV/cm and microwave power of 30 dBm. Figure 4(c) shows the dispersion curve of the resonance field $H_r$ with respect to frequency. By fitting it with Eq. (1), we get the gyromagnetic ratio $\gamma/2\pi = 28$ GHz/T and find that the effective saturation magnetization $M_{eff}$ is around 1.05 T for $Co_2FeSi$.

To investigate the continuous modulation of the charge-spin conversion of $Co_2FeSi$ alloy by the applied electric field,

we performed ST-FMR measurements at 7 GHz with different electric fields. We first plot the curves of the linewidth $\Delta H$ and the resonance field $H_r$ with the electric field, as shown in Figs. 5(a) and 5(b). It is found that the linewidth $\Delta H$ and resonance field $H_r$ vary in a butterfly-like shape with the electric field, which can be ascribed to the strain effect. In ferromagnetic/ferroelectric heterostructures, the strain effect is widely present. Through the piezoelectric effect, the electric field can modulate the lattice of ferroelectric materials. In addition, the resulting strain is transferred from the ferroelectric layer to the ferromagnetic layer with the magnetostriction effect, leading to the magnetoelectric coupling effect.[35–37] Therefore, the strain anisotropy energy is brought in, resulting in changes in the orbital polarization and electron density of the electronic states, enabling the modulation of the magnetization precession of $Co_2FeSi$.[19]

Moreover, the modulation of the electric field for the resonance field $H_r$ originates from the change in magnetic anisotropy due to strain effect, which makes contributions to the butter-like behavior of $\xi$ with the electric field. The above results indicate that the modulation of the dynamic magnetic properties of $Co_2FeSi$ alloy by the applied electric field.

Furthermore, we summarize the charge-spin conversion efficiency $\xi$ under different electric fields as shown in Fig. 5(c). By comparison, it is found that the following relationship exists between the charge-spin conversion efficiency $\xi$ in the remnant polarized and unpolarized states: $\xi_+ > \xi > \xi_-$, which illustrates that there is a controllable modulation of the charge-spin conversion efficiency by the electric field. Moreover, the charge-spin conversion efficiency shows butterfly-like behavior with the electric field, which is compatible with the strain curve ($S$–$E$) of the ferroelectric substrate PMN-PT, indicating the modulation of the charge-spin conversion efficiency by the piezoelectric strain effect. Theoretically, the first-principles calculations were exploited and we found that the modulation of SOTs by the electric field originates from the unique change in the orbital polarization of the electronic states caused by lattice distortion. The work revealed the microscopic origin of the piezoelectric strain effect affecting SOTs. Since piezoelectric strain is locally generated, non-volatile magnetic state modulation can be achieved by pulsed electric fields, which greatly accelerates the development of new spintronics devices with high-density storage, low-power consumption, and high speed.

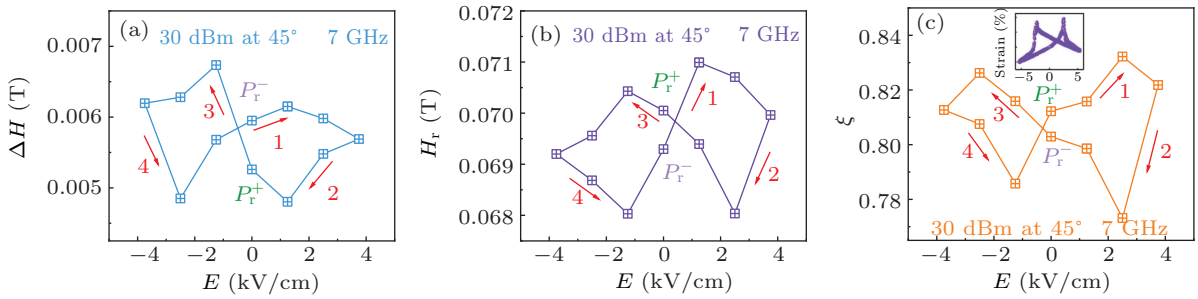



**Fig. 5.** (a) Variation curve of line width $\Delta H$ with electric field at 7 GHz and 30 dBm. (b) Variation curve of resonance field $H_r$ with electric field at 7 GHz and 30 dBm. (c) Variation curve of charge-spin conversion efficiency $\xi$ with electric field at 7 GHz and 30 dBm.

## 4. Conclusion

In conclusion, the strain response to charge-spin conversion in Pt/$Co_2FeSi$/PMN-PT has been experimentally investigated. We can modulate the dynamic magnetic properties and charge-spin conversion efficiency $\xi$ of the $Co_2FeSi$ alloy through an applied electric field by employing ST-FMR. The results show that the $\xi$ exhibits butterfly-like behavior with the electric field, which is consistent with the strain curve of the (001) oriented PMN-PT and could be attributed to piezostrain effect. The possibility of tuning charge-spin conversion at room temperature offers an alternative path for applications of such as spintronics devices and current-sensing magnetization switching.

## Acknowledgements

Project supported by the National Natural Science Foundation of China (Grant No. 11974149) and the Natural Science Foundation of Gansu Province (Grant No. 21JR7RA472).

## References

[1] Manchon A, Železny J, Miron I M, Jungwirth T, Sinova J, Thiaville A, Garello K and Gambardella P 2019 *Rev. Mod. Phys.* **91** 035004
[2] Hirsch J E 1999 *Phys. Rev. Lett.* **83** 1834
[3] Shao Q, Yu G, Lan Y W, Shi Y, Li M Y, Zheng C, Zhu X, Li L J, Amiri P K and Wang K L 2016 *Nano Lett.* **16** 7514
[4] Ramaswamy R, Lee J M, Cai K and Yang H 2018 *Appl. Phys. Rev.* **5** 031107
[5] Kim J, Sinha J, Hayashi M, Yamanouchi M, Fukami S, Suzuki T, Mitani S and Ohno H 2013 *Nat. Mater.* **12** 240
[6] Garello K, Miron I M, Avci C O, Freimuth F, Mokrousov Y, Blügel S, Auffret S, Boulle O, Gaudin G and Gambardella P 2013 *Nat. Nanotechnol.* **8** 587
[7] Liu L, Pai C F, Li Y, Tseng H W, Ralph D C and Buhrman R A 2012 *Science* **336** 555
[8] Schulz T, Lee K, Krüger B, Conte R Lo, Karnad G V, Garcia K, Vila L, Ocker B, Ravelosona D and Kläui M 2017 *Phys. Rev. B* **95** 224409
[9] Manchon A, Koo H C, Nitta J, Frolov S M and Duine R A 2015 *Nat. Mater.* **14** 871
[10] Brataas A, Tserkovnyak Y, Bauer G E W and Halperin B I 2002 *Phys. Rev. B* **66** 060404

[11] Azzawi S, Ganguly A, Tokaç M, Rowan-Robinson R M, Sinha J, Hindmarch A T, Barman A and Atkinson D 2016 *Phys. Rev. B* **93** 054402

[12] Kumar A, Akansel S, Stopfel H, Fazlali M, Akerman J, Brucas R and Svedlindh P 2017 *Phys. Rev. B* **95** 064406

[13] Barati E and Cinal M 2017 *Phys. Rev. B* **95** 134440

[14] Yang H, Li Y and Bailey W E 2016 *Appl. Phys. Lett.* **108** 242404

[15] Jiang C, Wang F, Dong C, Zhou C, Wu L and Xue D 2016 *Appl. Phys. Lett.* **108** 032401

[16] Dong C, Guo D, Wu L, Wang F, Jiang C, Jia C and Xue D 2014 *Appl. Phys. Lett.* **104** 062403

[17] Wu L, Zhang C, Dong C, Jia C, Jiang C and Xue D 2015 *Appl. Phys. Lett.* **107** 122905

[18] Lv W, Jia Z, Wang B, Lu Y, Luo X, Zhang B, Zeng Z and Liu Z 2018 *ACS Appl. Mater. Interfaces* **10** 2843

[19] Filianina M, Hanke J P, Lee K, Han D S, Jaiswal S, Rajan A, Jakob G, Mokrousov Y and Klaeui M 2020 *Phys. Rev. Lett.* **124** 217701

[20] Cai K, Yang M, Ju H, Wang S, Ji Y, Li B, Edmonds K W, Sheng Y, Zhang B, Zhang N, Liu S, Zheng H and Wang K 2017 *Nat. Mater.* **16** 712

[21] Trudel S, Gaier O, Hamrle J and Hillebrands B 2010 *J. Phys. D: Appl. Phys.* **43** 193001

[22] De Groot R A, Mueller F M, Van Engen P G and Buschow K H J 1983 *Phys. Rev. Lett.* **50** 2024

[23] Oogane M, Yilgin R, Shinano M, Yakata S, Sakuraba Y, Ando Y and Miyazaki T 2007 *J. Appl. Phys.* **101** 09J501

[24] Ramaswamy R, Lee J M, Cai K and Yang H 2018 *Appl. Phys. Rev.* **5** 031107

[25] Wang Y, Ramaswamy R and Yang H 2018 *J. Phys. D: Appl. Phys.* **51** 273002

[26] Yang W L, Wei J W, Wan C H, Xing Y W, Yan Z R, Wang X, Fang C, Guo C Y, Yu G Q and Han X F 2020 *Phys. Rev. B* **101** 064412

[27] Liu L, Moriyama T, Ralph D C and Buhrman R A 2011 *Phys. Rev. Lett.* **106** 036601

[28] Nan T, Emori S, Boone C T, Wang X, Oxholm T M, Jones J G, Howe B M, Brown G J and Sun N X 2015 *Phys. Rev. B* **91** 214416

[29] Liu L, Pai C F, Li Y, Tseng H W, Ralph D C and Buhrman R A 2012 *Science* **336** 555

[30] Pai C F, Liu L, Li Y, Tseng H W, Ralph D C and Buhrman R A 2012 *Appl. Phys. Lett.* **101** 122404

[31] Wang Y, Ramaswamy R, Motapothula M, Narayanapillai K, Zhu D, Yu J, Venkatesan T and Yang H 2017 *Nano Lett.* **17** 7659

[32] Wang Y, Deorani P, Banerjee K, Koirala N, Brahlek M, Oh S and Yang H 2015 *Phys. Rev. Lett.* **114** 257202

[33] Mellnik A R, Lee J S, Richardella A, Grab J L, Mintun P J, Fischer M H, Vaezi A, Manchon A, Kim E A, Samarth N and Ralph D C 2014 *Nature* **511** 449

[34] Yu D, Luo S, Li Y, Koval V and Jia C 2019 *Phys. Rev. B* **100** 104410

[35] Zhang C, Wang F, Dong C, Gao C, Jia C, Jiang C and Xue D 2015 *Nanoscale* **7** 4187

[36] Zhang S, Zhao Y G, Li P S, Yang J, Rizwan S, Zhang J, Seidel J, Qu T, Yang Y J, Luo Z L, He Q, Zou T, Chen Q P, Wang J W, Yang L F, Sun Y, Wu Y Z, Xiao X, Jin X F, Huang J, Gao C, Han X F and Ramesh R 2012 *Phys. Rev. Lett.* **108** 137203

[37] Jiang C, Zhang C, Dong C, Guo D and Xue D 2015 *Appl. Phys. Lett.* **106** 122406